

**Title:**

Altered resting-state whole-brain functional networks of neonates with intrauterine growth restriction

**Authors:**

Dafnis Batalle<sup>a,b,1</sup>, Emma Muñoz-Moreno<sup>a</sup>, Cristian Tornador<sup>c</sup>, Nuria Bargallo<sup>d,e</sup>,  
Gustavo Deco<sup>c,f</sup>, Elisenda Eixarch<sup>a,g,h</sup>, Eduard Gratacos<sup>a,g,h</sup>

**Affiliations:**

- a) Fetal and Perinatal Medicine Research Group, Institut d'Investigacions Biomediques August Pi i Sunyer (IDIBAPS), Barcelona, Spain
- b) Centre for the Developing Brain, Division of Imaging Sciences & Biomedical Engineering, King's College London, London, United Kingdom
- c) Center for Brain and Cognition, Computational Neuroscience Group, Department of Information and Communication Technologies, Universitat Pompeu Fabra, Barcelona, Spain
- d) Department of Radiology, Centre de Diagnòstic per la Imatge Clínic (CDIC), Hospital Clínic, Barcelona, Spain
- e) Magnetic Resonance core facility, Institut d'Investigacions Biomediques August Pi i Sunyer (IDIBAPS), Barcelona, Spain
- f) Institució Catalana de la Recerca i Estudis Avançats (ICREA), Universitat Pompeu Fabra, Barcelona, Spain
- g) Maternal-Fetal Medicine Department, ICGON, Hospital Clínic, Universitat de Barcelona, Barcelona, Spain
- h) Centro de Investigación Biomédica en Red de Enfermedades Raras (CIBERER), Barcelona, Spain

**Corresponding author:**

<sup>1</sup> Dafnis Batalle

Fetal and Perinatal Medicine Research Group, Hospital Clínic – IDIBAPS  
Sabino de Arana 1, Helios III, 08028 Barcelona, Spain  
Phone: +34 932 275 400 ext. 7286  
Email: [dbatalle@clinic.ub.es](mailto:dbatalle@clinic.ub.es)

**ABSTRACT**

The feasibility to use functional MRI (fMRI) during natural sleep to assess low-frequency basal brain activity fluctuations in human neonates has been demonstrated, although its potential to characterise pathologies of prenatal origin has not yet been exploited. In the present study, we used intrauterine growth restriction (IUGR) as a model of altered neurodevelopment due to prenatal condition to show the suitability of brain networks to characterise functional brain organisation at neonatal age. Particularly, we analysed resting-state fMRI signal of 20 neonates with IUGR and 13 controls, obtaining whole-brain functional networks based on correlations of BOLD signal in 90 grey matter regions of an anatomical atlas (AAL). Characterisation of the networks obtained with graph theoretical features showed increased network infrastructure and raw efficiencies but reduced efficiency after normalisation, demonstrating hyper-connected but sub-optimally organised IUGR functional brain networks. Significant association of network features with neurobehavioral scores was also found. Further assessment of spatiotemporal dynamics displayed alterations into features associated to frontal, cingulate and lingual cortices. These findings show the capacity of functional brain networks to characterise brain reorganisation from an early age, and their potential to develop biomarkers of altered neurodevelopment.

**Keywords:**

*brain mapping, fMRI, newborn, fetal growth retardation, connectomics*

**Abbreviations:**

ADHD: attention deficit hyperactive disorder; ASD: autism spectrum disorders; BOLD: blood oxygen level-dependent; CSF: cerebrospinal fluid; DFC: dynamic functional connectivity; FA: fractional anisotropy; FDR: false discovery rate; GA: gestational age; GM: grey matter; ICA: independent component analysis; IUGR: Intrauterine growth restriction; MRI: Magnetic resonance imaging; NBAS: Neonatal Behavioral Assessment Scale; PMA: post menstrual age; ROI: region of interest; rs-fMRI: resting-state functional MRI; RSN: resting state networks; WM: white matter.

## 1. INTRODUCTION

Intrauterine growth restriction (IUGR) affects 5-10% of all pregnancies in developed countries and it is a major public health issue, being associated with short- and long-term neurodevelopmental and cognitive dysfunctions (Arcangeli, Thilaganathan, Hooper, Khan, & Bhide, 2012; Baschat, 2013; Løhaugen et al., 2013). The characterisation of underlying brain alterations supporting these dysfunctions and the prediction of the subset of the population with a higher risk of altered neurodevelopmental outcomes are among the challenges of modern fetal medicine and paediatrics. Magnetic resonance imaging (MRI) has been used to characterise structural brain alterations underlying neurodevelopmental dysfunctions of subjects with IUGR at different stages of development, starting in-utero (Egaña-Ugrinovic, Sanz-Cortes, Figueras, Bargallo, & Gratacos, 2013; Sanz-Cortes et al., 2013), persisting at neonatal and early infancy (De Bie et al., 2011; Dubois et al., 2008; Esteban et al., 2010; Lodygensky et al., 2008; Padilla et al., 2011; Tolsa et al., 2004) and at adolescence (Martinussen et al., 2009; Skranes et al., 2005). In the recent years, the knowledge of structural brain organisation has significantly advanced with the assessment of the macroscopic circuitry of connections of the brain with structural brain networks obtained from MRI (Hagmann, 2005; Sporns, Tononi, & Kotter, 2005). Importantly, graph theoretical features have been used to characterise brain networks (Bullmore & Sporns, 2009), allowing to comprehensibly describe with a few network features the underlying brain connectivity organisation. This approach has been demonstrated to be useful to characterise a wide-range of pathologies and conditions that affect brain connectivity (Bassett & Bullmore, 2009). Based on anatomical and diffusion MRI, this technique has been promising in the study of IUGR, allowing to demonstrate alterations in the structural brain network organisation and its association with altered neurodevelopment in one-year-old infants (Batalle et al., 2012; Batalle et al., 2013), school-age infants (Fischi-Gomez et al., 2014), and in an animal model of long-term IUGR (Batalle et al., 2014). However, it remains unknown if there is brain reorganisation at a functional level in this population, and if it can be detected at neonatal age.

Since the seminal study of Biswal et al. (Biswal, Yetkin, Haughton, & Hyde, 1995), the potential of low-frequency components of resting-state functional MRI (rs-fMRI) to obtain whole-brain functional brain networks based on partial correlations of blood oxygen level-dependent (BOLD) signal (Salvador et al., 2005) has been demonstrated. Several studies have demonstrated the feasibility to use rs-fMRI to characterise the functional organisation of the healthy neonatal brain, opening the opportunity to characterise also the alterations in brain organisation due to prenatal conditions, such as IUGR. Using independent component analysis (ICA), the emergence of synchronised spontaneous low-frequency rs-fMRI BOLD signals exhibiting resting state networks (RSN) has been demonstrated in term and preterm infants during light sedation and natural sleep (Fransson et al., 2009; Fransson et al., 2007). Both ICA and seed-based correlation approaches have also been used in longitudinal studies showing the emergence of connections partially or completely matching several RSN during neonatal development (Doria et al., 2010; Gao et al., 2009; Lin et al., 2008; Smyser et al., 2010). However, studies considering whole-brain functional brain networks of the neonatal brain are scarce in the literature. Neonatal networks composed of selected regions of interest (ROIs) were studied by Gao et al. (2009), while voxel-wise networks obtained in a normalised space were obtained by Fransson et al. (Fransson, Aden, Blennow, & Lagercrantz, 2011), showing the presence of cortical hubs and sub-networks associated with these hubs. Finally, Gao et al. (2011) studied the normal evolution of ROI-based functional brain networks from neonatal age to two years of age and its resilience to random attacks, and recently van den Heuvel et al. (2015) studied the evolution of both structural and functional connectivity during preterm brain development.

In the present study we used partial correlations of rs-fMRI BOLD signals averaged into 90 regions of an anatomical brain atlas (Tzourio-Mazoyer et al., 2002) in 13 controls and 20 subjects with IUGR scanned around 44 weeks equivalent post menstrual age (PMA). Using the whole-brain functional networks obtained we characterised alterations in the individual functional brain connectivity of neonates with IUGR using graph theory features. We further characterised functional spatiotemporal dynamics and assessed network nodes with altered temporal characteristics.

Finally, the association of individual network features with neonatal neurobehavioral outcomes was also assessed.

ACCEPTED MANUSCRIPT

## 2. MATERIAL AND METHODS

### 2.1 Participants, neurobehavioral assessment and MRI acquisition

The infants of the study were part of a larger prospective research program in IUGR involving fetal assessment and short- and long-term postnatal follow-up at Hospital Clínic (Barcelona, Spain). The local Ethics Committee approved the study protocol, and written informed consent was obtained from the parents or legal guardians of all the participants (CEIC: 2012/7715). The original sample of the study included a sample of 45 pregnancies with 30 late-onset IUGR and 15 control fetuses. Late-onset IUGR was defined as those fetuses with estimated fetal weight below the 10<sup>th</sup> centile according to local reference standards (Figueras et al., 2008) confirmed at birth and delivered after 34 weeks of pregnancy. Control subjects were sampled from general pregnant population and defined as fetuses with fetal estimated weight between 10<sup>th</sup> and 90<sup>th</sup> centile confirmed at birth. Infants with chromosomal, genetic or structural defects and signs of intrauterine infection or neonatal onset sepsis were excluded from the study. Neonatal data was prospectively recorded including gestational age (GA), birth weight, gender, Apgar at 5 min, umbilical artery pH, neonatal complications and maternal smoking status during pregnancy.

MRI was performed around one month corrected age during natural sleep after feeding the baby. An expert neuroradiologist analysed anatomical images and those infants without overt brain lesions were further analysed. In addition, all acquired images were visually inspected for apparent artefacts and subjects excluded accordingly. Thus, ten of 30 cases and two of the 15 controls were excluded from the study due to white matter (WM) lesions, awakening or excessive movement during acquisition, obtaining a final sample of 13 controls (5 males) and 20 subjects with IUGR (13 males). Characteristics of the population are described in Table 1. Particular care was taken in order to ensure neonatal welfare during the MR acquisition. A pulseoximetry probe was placed around the baby's wrist to monitor oxygen saturation levels throughout the scan, and acoustic noise was minimised with the use of neonatal ear muffs (MiniMuffs ® Neonatal Noise Attenuators, Natus Medical Incorporated, USA). The infant was swaddled with one or two infant sheets before being placed within a vacuum immobiliser, air was removed from the bag and the infant was contained

within a rigid cradle that is shaped to its body, effectively swaddling the infant. The lighting in the scanner room was reduced to aid the infant's sleep but was kept at a level that allows safely monitoring.

Neonatal neurobehavioral performance was assessed at neonatal age with the Neonatal Behavioral Assessment Scale (NBAS) (Nugent & Brazelton, 2000), which evaluates cortical and subcortical functions in 35 items grouped into 6 clusters: habituation, social-interactive, organisation of state, regulation of state, autonomous nervous system and attention (Sagiv et al., 2008). Cluster scores were transformed to z-scores according to a standard population (Costas Moragas, Fornieles Deu, Botet Mussons, Boatella Costa, & de Caceres Zurita, 2007; Sagiv et al., 2008) and defined as abnormal if they have a z-score below minus one. NBAS severity score was defined as the number of abnormal NBAS clusters for each subject. Due to the low successful rate of a valid habituation cluster (12 out of 33), it was excluded from the calculation of NBAS severity score. Therefore, severity score was only calculated on 29 out of 33 subjects that had valid estimation of social-interactive, organisation of the state, regulation of the state, autonomous nervous system and attention clusters, in a range from 0 to 5.

## 2.2 MRI acquisition

MRI acquisition was performed with a TIM TRIO 3.0 T whole body MR scanner (Siemens, Germany). Anatomical T2-weighted acquisition consisted in 45 axial slices with 2-mm slice thickness, in-plane acquisition matrix of 256 x 256, FOV = 160 x 160 mm<sup>2</sup>, resulting in a resolution of 0.625 x 0.625 x 2 mm<sup>3</sup>, TR = 5460 ms and TE = 91 ms. Functional MRI data were acquired using gradient EP) consisting in volumes of 42 axial slices with 2-mm slice thickness, in-plane acquisition matrix of 80 x 80, FoV = 160 x 160 mm<sup>2</sup>, yielding a spatial resolution of 2 x 2 x 2 mm<sup>3</sup>, TR = 2000 ms, TE = 20 ms. Resting-state functional connectivity was assessed during 8 minutes of natural sleep (240 EPI volumes). The first ten volumes were discarded to allow accommodating T1-equilibrium processes, and we only consider the remaining 230 volumes for further analysis. The acquisition protocol included other sequences not used in this study, having a total scanning time of ~30-45 min.

### 2.3 Pre-processing and network extraction

All anatomical T2-weighted volumes were first skull-stripped using BET (Smith, 2002). Brain tissue was segmented into WM, grey matter (GM) and cerebrospinal fluid (CSF) with unified segmentation model (Ashburner & Friston, 2005) available with SPM8. The default adult templates were replaced with specific neonatal tissue probability maps (Shi et al., 2011). AAL atlas (Tzourio-Mazoyer et al., 2002) recently adapted to neonatal population in a T2-weighted template (Shi et al., 2011) was used to parcellate each subject into 90 cortical and sub-cortical regions (Supplementary Table 1). Particularly, a customised software implementing a consistent version (Tristan-Vega & Arribas, 2007) of a block matching algorithm (Warfield et al., 2002) was used to obtain an elastic transformation matching the template with each subject's T2 volume. AAL labels were propagated to each subject using this elastic transformation with discrete labelling preserved by nearest neighbour interpolation.

Image pre-processing of BOLD images was mainly performed with SPM8 package. First, intra-volume time differences between slices were corrected. Inter-volume geometric displacements were corrected using a six-parameter rigid transformation for each acquired volume and spatially smoothed using a Gaussian kernel with 2 mm full width at half maximum. Correction of head motion effects in the signal was performed by regressing out the 6-parameter head motion profiles previously estimated in each voxel across all the acquisition time. Root mean square frame displacement (FD-RMS) between each volume was estimated using average of rotation and translation parameters differences (Power, Barnes, Snyder, Schlaggar, & Petersen, 2012) using matrix RMS formulation, as available in FSL5.0 Motion Outliers tool. Number of outliers in each subject ( $>75^{\text{th}}$  percentile +  $1.5 \times$  InterQuartile Range) was also recorded. GM/WM/CSF segmentation and AAL ROI parcellation obtained in T2 anatomical volume were registered to an averaged BOLD volume using an affine transformation. The representative averaged time series corresponding to each ROI were estimated for those voxels belonging to the GM mask and band pass filtered (0.01 – 0.15 Hz). This “broad band” has been suggested to be the more reliable for graph theory analysis (Braun et al., 2011). Network edges were calculated as the partial correlation



coefficients obtained between each pair of ROI averaged signal excluding the effects of the signal of the other 88 ROIs, obtaining a 90 x 90 partial correlation matrix for each subject. Pearson coefficients were transformed according to Fisher z-transformation and negative correlation coefficients were excluded, i.e., thresholding the networks with  $\rho > 0$ . The correlation between each pair of ROIs excluding the effect of the signal common to the rest of ROIs was therefore inferred to be proportional to the connectivity of each given pair of ROIs, obtaining weighted matrices that represent the raw connectivity of RSN of each subject, as shown in Figure 1A. Note that only positive correlations were included

## 2.4 Network normalisation

In order to disentangle network infrastructure from network organisation, i.e., evaluate the organisation of networks independently of their average strength and density (cost), three different approaches were followed. First, different average strength among subjects was neutralised by means of normalisation of each subject's brain network by its total energy (Batalle et al., 2014), that is, given a network  $C$  with weights  $w_{i,j}$  for each pair of nodes  $i, j$ , we defined a normalised version of the network  $C^{norm}$  with normalised weights defined as  $w_{i,j}^{norm} = w_{i,j} / \sum_{\forall i,j} w_{i,j}$ . Secondly, differences of network density (cost) were neutralised by means of a cost-corrected analysis of network features (Achard & Bullmore, 2007). Following this approach, a binary network was created at different network costs, selecting for each cost-value  $x$  the connections with a strongest weight that yield to a cost  $x$ . The cost range was limited by the minimum value of network density for any subject included into the analysis, which is the maximum network cost where is possible to fairly compare among all the subjects. Finally, the effect of differences in strength and density were neutralised at the same time by means of a combination of both methods: instead of obtaining a binary network at each network cost, as it was performed in the second approach, the weighted network obtained at each network cost was considered in this third approach. Given that weighted features are much related to the strength of a network (weighted cost), to obtain pure organisational descriptors, the weighted networks obtained at each network cost were normalised as described in the strength normalisation approach. Particularly, for a given network  $C(i,j) = w_{i,j}$  where  $w_{i,j}$

represents the weight of the connection between nodes  $i$  and  $j$ , we defined a cost-corrected network  $C_w(i, j, x)$  for each value of cost  $x$ . Note that  $C_w(i, j, x) = w_{i,j}(x)$  where  $w_{i,j}(x) = w_{i,j}$  if the link between node  $i$  and  $j$  belongs to the subset of strongest connections that ensure a network density of  $x$  and  $w_{i,j}(x) = 0$  otherwise. In this context, normalised cost-corrected network at cost  $x$  was defined as  $C_w^{norm}(i, j, x) = w_{i,j}(x) / \sum_{i,j} w_{i,j}(x)$ .

## 2.5 Network analysis

Graph theory features allow summarising infrastructure and organisation of a brain network represented as an adjacency matrix (binary or weighted). Global functioning of each network was assessed by its infrastructure (average strength), integration (global efficiency) and segregation (local efficiency). Regional characteristics were evaluated by means of nodal strength, assessing the total connectivity of a node in a given network, and nodal efficiency, measuring the efficiency of the sub-network associated to a given node. Nodes with a high nodal efficiency indicate a high tolerance of the network to the elimination of the given node, which is associated to a high clustering of the neighbourhood of this node (Achard & Bullmore, 2007). Formulation and calculation of the graph theory features used to assess each network was based on the definitions and code compiled by Rubinov and Sporns (Rubinov & Sporns, 2009).

## 2.6 Dynamic functional connectivity

Dynamic functional connectivity (DFC) has been defined as the functional connectivity over a sliding time window (Sakoglu et al., 2010). Recently, phase synchronisation has been used to solve the resolution/reliability trade-off of windowing the signal in functional MRI time-series by means of conversion of the real signal into a complex analytic version, with techniques such as Hilbert transform. In the present study, we used similar techniques to study the temporal dynamics of the ROI signals in a narrowband (0.04-0.07 Hz) comparing phase differences pair-wise and obtaining a measure of phase similarity between each pair of ROIs at each instant of time. Narrowband filtering of the signal allows the application of the Hilbert transform to extract the phases obtaining an analytic signal (Glerean, Salmi, Lahnakoski, Jaaskelainen, & Sams, 2012). This analytic signal

represent the narrowband signal  $s(t)$  as a rotating vector with an instant phase  $\varphi(t)$  and an instant amplitude  $A(t)$ , i.e.,  $s(t) = A(t)\cos(\varphi(t))$ . Phase of the signal was obtained from the complex signal  $z(t) = s(t) + i.H[s(t)]$ , where  $i$  is the imaginary unit and  $H[s(t)]$  is the Hilbert transform of  $s(t)$ . Global level of phase synchrony among all brain areas was quantified with Kuramoto order parameter  $R(t)$ , defined as  $R(t) = \left| \frac{1}{N} \sum_{j=1}^N e^{i\varphi_j(t)} \right|$ , where  $N$  is the number of ROIs. Kuramoto order parameter quantifies the level of global synchronisation of a collection of phase oscillators, being constrained between 0 and 1 increasing monotonically as a function of the level of global synchronisation between all pairs of ROIs in the system, 0 representing total asynchrony and 1 representing total synchrony. As Kuramoto order parameter is defined at each time point, describing the evolution of spatial coherence as a function of time, it was averaged across all time points in order to obtain a global feature characterising the average level of synchronisation of each subject.

Further analysis involved the calculation of a measure of phase similarity between each pair of regions for each instant of time. Hence, the level of synchronisation between a pair of brain areas was considered inversely proportional to their phase difference, giving them a weight  $w_{ij}^H(t)$  at each instant of time as  $w_{ij}^H(t) = \left| \frac{\Delta\varphi_{ij}(t) - \pi}{\pi} \right|$ . Note that as  $\Delta\varphi_{ij}(t)$  is constrained between 0 and  $\pi$ ,  $w_{ij}^H(t)$  will be constrained between 0 and 1, being  $w_{ij}^H(t) = 1$  when the phase of the two regions is identical. Using this approach, a weighted connectivity matrix based on the phase similarity was constructed at each instant of time, allowing the extraction of temporal-dependent global and regional network features that assess dynamic functional connectivity organisation.

However, given that the subjects are not receiving a specific stimulus that would allow direct correspondence with temporal points and specific brain state, features obtained at each time point are not easily comparable among subjects. Hence, we used Kuramoto order parameter to reorder temporal axis according to the relative level of global synchronisation of each subject, from its lowest to its highest level. Therefore, although after reordering we still cannot give interpretation to each time point, overall they can now be interpreted as a percentage of time points showing the

same percentage of synchronisation relative to each subject, this way it is possible to reorder the temporal features obtained for each subject and can be compared as they are obtained based on the same relative level of synchronisation.

## 2.7 Statistical analysis

Comparisons among groups were performed by general linear models (GLM) with gender and smoking status of the mother as a co-factor and GA and PMA at MRI as co-variables. Significance was declared at  $p < 0.05$  (uncorrected). Regional alterations were shown using BrainNet viewer (Xia, Wang, & He, 2013). Association of network features obtained with NBAS in IUGR group was performed by means of partial correlations using gender, GA and smoking status as confounder factors. The software package SPSS 21.0 (SPSS, Chicago, IL) was used for the statistical analyses. Computational algorithms were implemented using MATLAB (2009b, The MathWorks Inc., Natick, MA).

## 3. RESULTS

### 3.1 Resting-state networks in IUGR neonates

Infrastructure of the raw weighted partial correlation functional brain networks obtained (Figure 1B-D) was assessed by comparing weighted graph theoretical features among groups by means of GLM. Importantly, this analysis showed significantly increased values of IUGR average strength ( $p = 0.013$ ), suggesting an increased pattern of weighted connectivity in IUGR networks. As expected of more strongly connected networks, weighted measures of global ( $p = 0.015$ ) and local efficiency ( $p = 0.028$ ) were also increased in IUGR. Network density, however, did not significantly differ between cases and controls.

Analysis of the pure organisational components of brain networks is strongly influenced by differences in the network infrastructure among subjects (Ginestet, Nichols, Bullmore, & Simmons, 2011). In order to assess the effectiveness of the organisation between groups independently of average strength, the effect of different values of average strength among subjects was neutralised

by means of normalisation of each subject's brain network, as previously described in section 2.4. As a result, significantly reduced normalised local efficiency was observed in IUGR group ( $p=0.003$ , Figure 1E). Although non significantly different between IUGR and control group, differences among subjects in network density (cost) could also be influencing the analysis of network organisation when using global network features. In this case, this effect was neutralised by means of a cost-corrected analysis (Achard & Bullmore, 2007), obtaining binary global and local efficiency features at each network cost from 0 to 0.51 at 0.01 steps. The maximum value of the range was fixed at 0.51 as it is the lower network density for any subject included. Using this approach, IUGR showed significantly reduced values for several costs (Figure 1F-G), and importantly, when integrated among the whole valid cost-range (Ginestet et al., 2011), significantly reduced global efficiency ( $p=0.008$ ) and local efficiency ( $p=0.013$ ) were also observed. Finally, differences in strength and network density were neutralised simultaneously by means of a combination of both methods (see Material and Methods). This way, the optimal distribution of weights in the network, i.e., the importance of having strong connections in key regions from a network topology point of view can be assessed independently of the influence of differences in average strength and network density at the same time. Using this approach, reduced values for cost-corrected weighted global and local efficiency were observed at several network costs (Figure 1H-I), being their cost-integrated values also significantly reduced for global and local efficiencies ( $p=0.013$  and  $p=0.016$  respectively). All three different approaches of normalisation yielded the same conclusion: although IUGR had an increased RSN infrastructure characterised by increased average strength yielding to increased raw efficiencies, its organisation was sub-optimal when compared with controls.

In addition to the analysis of global network features, in order to find the regional components that have a higher influence in the network reorganisation observed in IUGR group, differences among groups were assessed using a GLM for each nodal feature using a similar approach as previously used for global network features. Particularly, nodal strength and nodal efficiency were further assessed in its raw and normalised versions (Figure 2). We observed that nodal features of raw networks showed a pattern of alterations in IUGR for both nodal efficiency and strength in frontal areas, but also on occipital, parietal and sub-cortical regions. Nodal strength and efficiency

of normalised networks showed a reduced number of alterations in IUGR, although there were still present some significant differences in subnetworks belonging to frontal, temporal and occipital cortices and sub-cortical regions such as amygdala and hippocampus. Note, however, that the nodal alterations reported must be considered exploratory, given that the differences observed did not withstand a false discovery rate (FDR) correction (Benjamini, Krieger, & Yekutieli, 2006).

### 3.2 Dynamic functional connectivity

In order to assess if there were any notable differences in the DFC of IUGR, we first used Kuramoto order parameter  $R$  to analyse the global level of synchronisation of each subject's brain at each instant of time (Figure 3A), being zero for complete asynchrony and 1 for full synchronisation. As the subject's acquisition was not under specific stimuli, rather than analysing the results in a temporal basis, the average value over time was compared. A tendency towards significance of having an increased Kuramoto order parameter was observed in IUGR group ( $p=0.055$ ), showing that, overall, subjects with IUGR tend to present a more synchronised brain than their control counterparts. The Kuramoto order parameter was further used to sort the acquisition time-points of each individual subject, from the lowest to the highest level of synchronisation of each subject's whole-brain DFC. This allowed comparing the temporal dynamics among subjects at a similar level of synchronisation given a temporal instant. Particularly, we observed significantly increased values of Kuramoto order parameter for several time points in IUGR (Figure 3B), and as expected, increased global and local efficiency for several time points (Figure 3C-D). Differences of nodal efficiency among groups at each instant of time were also assessed, finding a set of nodes with statistically significant differences in IUGR across time (Figure 3E). Observing the percentage of time that each nodal efficiency is significantly different in IUGR allowed highlighting four regional features altered in IUGR more than two standard deviations above the mean: left superior frontal gyrus dorsolateral part (F1-L), right middle frontal gyrus, orbital part (F2O-R), right median cingulate and paracingulate gyri (MCIN-R), and left lingual gyrus (LIN-L). Analogous analysis of nodal strength yielded similar results, in this case being only left superior

frontal gyrus, dorsolateral part (F1-L) and right middle frontal gyrus, orbital part (F2O-R) the regions found to be different during a significant amount of time.

### 3.3 Association with neonatal neurobehavior

Neonatal behavioral assessment scale (NBAS) (Nugent & Brazelton, 2000) was used to characterise neurobehavioral outcomes in neonatal period. Association of neurobehavioral scores (NBAS) with global network features (average strength, network density, weighted global and local efficiency, normalized global and local efficiency, binary cost-integrated global and local efficiency and weighted normalised cost-integrated global and local efficiency) was assessed by means of partial correlations controlling for weight centile, gender, GA and smoking status. Hence, network density (i.e., the amount of connections over the total amount possible) was found to be significantly correlated with social-interactive cluster ( $\rho=0.409$ ,  $p=0.042$ ) and attention cluster ( $\rho=0.523$ ,  $p=0.006$ ). Normalised weighted global efficiency was correlated with organisation of the state ( $\rho=0.434$ ,  $p=0.027$ ).

An ordinal regression of NBAS severity score (dependent variable) with main clinical data (GA, weight centile, gender and smoking status during pregnancy) was performed, yielding to a non-significant model ( $p=0.334$ ,  $\text{Chi}^2=4.570$ , Nagelkerke  $R^2=0.149$ ,  $df=4$ ). However, the addition of global network features (average strength, network density, weighted global and local efficiency, normalized global and local efficiency, binary cost-integrated strength, binary cost-integrated global and local efficiency and cost-integrated weighted normalised global and local efficiency) significantly changed the model ( $p=0.003$ ,  $\text{Chi}^2=28.692$ ,  $df=11$ ), allowing to obtain a statistically significant model ( $p=0.004$ ,  $\text{Chi}^2=33.262$ , Nagelkerke  $R^2=0.706$ ,  $df=15$ ), showing significant association of graph theory features based on RSN with the severity of abnormal neurobehavioral outcomes and the addition of significant information to main clinical features.

#### 4. DISCUSSION

Characterisation of the brain changes underlying neurodevelopmental problems in IUGR is a current challenge in modern fetal and paediatric medicine (Ment, Hirtz, & Huppi, 2009). A better understanding of the pathophysiology of this condition is essential to start developing early biomarkers to detect the infants at high risk of having altered neurodevelopmental problems. Importantly, it has been shown that early individualised interventions significantly improves IUGR neurobehavioral performance at short- and mid-term (Als et al., 2012; McAnulty et al., 2013). However, given the high prevalence of IUGR and the economic cost of individualised care units, selecting those IUGR infants with a higher risk is essential to appropriately advise parents and optimally use clinical resources. With this long-term goal in mind, in the present study we investigated functional brain networks in IUGR.

The results obtained showed a very specific pattern of alterations in IUGR whole-brain RSN, characterised by a hyper-connectivity of their raw networks. However, when assessing the pure organisational features by means of three different normalisation procedures, we observe a sub-optimal organisation in IUGR characterised by decreased global and local efficiency. Further analysis of nodal features showed a spread pattern of regional alterations in IUGR, however, not strong enough to withstand a FDR correction. Spatio-temporal analysis of the signal supported previous results, revealing a tendency of increased overall synchronisation in IUGR, and a set of nodal features that might have an important role in the reorganisation of functional brain networks obtained. These results, together with previously reported alterations in IUGR structural brain networks (Batalle et al., 2012) support the hypothesis that IUGR is a condition strongly associated with brain organisation, as has been suggested to happen with mood and psychiatric disorders. Albeit it is important to note that establishing a causality with the evidence available is still premature, association of network features with neurobehavioral performance is reported in this and other studies (Batalle et al., 2012; Batalle et al., 2013), postulating IUGR as a candidate to be a brain-network disorder (Rubinov & Bullmore, 2013).



Interestingly, in a previous study of structural brain networks in one-year-old population, reduced fractional anisotropy (FA) weighted global and local efficiency was found in IUGR (Batalle et al., 2012). Intuitively one would expect to obtain reduced efficiencies in functional brain networks due to a weaker structural connectivity, but in contrary, significantly increased raw efficiencies were found in IUGR neonates. A possible explanation for this discord could be the difference of age in the population under study, as it is a critical period in terms of brain connectivity changes (Yap et al., 2011). Although the constraining of functional connectivity to the structural substrate has been demonstrated (Deco et al., 2013; Honey et al., 2009; van den Heuvel et al., 2015), functional and structural brain networks might also be capturing different aspects of brain organisation, and they do not necessarily need to behave in the same manner (Cabral, Hugues, Kringelbach, & Deco, 2012; Cabral, Kringelbach, & Deco, 2012). Note also that in a previous study on healthy infants, Gao et al. (2011) showed that, from neonatal age to one year of age, more connections presented a reduction of connectivity than those presenting an increase. Thus we cannot discard a possible retard in maturation as an explanation of the general increase in IUGR average strength.

IUGR has been suggested to be a risk factor of developing disorders such as attention deficit hyperactive disorder (ADHD) (Heinonen et al., 2010; Linnet et al., 2006), autism spectrum disorders (ASD) (Gardener, Spiegelman, & Buka, 2011; Moore, Kneitel, Walker, Gilbert, & Xing, 2012) and schizophrenia (Nielsen et al., 2013). Although there are some contradictory reports, generally ASD has been characterised by having functional hyper-connectivity of salience and default mode network (Menon, 2013). However, whole-brain RSN have been reported to show reduced raw local efficiency but increased global efficiency after cost-correction (Rudie et al., 2012). In adult schizophrenia patients, reduced global and local efficiency after cost-correction of RSN has been reported (Liu et al., 2008), but also decreased average functional connectivity (Lynall et al., 2010). RSN of children with ADHD have been reported to have increased local efficiency for several costs, although raw weighted measures have not been described (Wang et al., 2009). Overall, after comparison with the body of literature we note a unique pattern of alterations in neonatal IUGR brain networks. This pattern of alterations must be confirmed at a later age, being the follow-up of IUGR population a crucial aspect for the characterisation of the evolution of the alterations and

long-term effects of this condition. The specific connectivity fingerprint trajectories that could underlie the increased prevalence of IUGR subjects developing disorders of neural development are not clear, and will be the likely focus of future prospective studies. We hypothesise that some of the links of IUGR with neurodevelopmental disorders could be partially associated with dysfunctions in some specific regional sub-networks produced by brain reorganisation. It is worthwhile to note that although partial correlation networks and temporal dynamics yield to same global functioning conclusions (IUGR has a hyper-connected, hyper-synchronised brain but with a sub-optimal organisation), the regional results obtained by each of these techniques showed different altered regions, suggesting that they assess complementary features of brain organisation, although both highlighted the role of frontal areas. Particularly, analysis of temporal dynamics allowed to obtain a reduced set of regions altered, comprised by frontal, cingulate and lingual cortices. In agreement with the results obtained, several frontal regions with altered structural brain network features have been previously reported in IUGR (Batalle et al., 2012), while evidence of alterations in frontal-posterior networks in ASD has been reported in several studies (Maximo, Cadena, & Kana, 2014). Interestingly, altered nodal efficiency of left lingual gyrus has been specifically reported in structural brain networks of IUGR (Batalle et al., 2012; Batalle et al., 2013) and has also been shown to be decreased in RSN of ADHD patients (Wang et al., 2009). Concerning cingulate cortical areas, FA measures of this area have been strongly associated with altered neurobehavioral performance in a long-term rabbit model of IUGR (Illa et al., 2013). In addition, functional alterations of cingulate areas have been reported in different studies of ASD (Maximo et al., 2014), schizophrenia (Lynall et al., 2010) and ADHD (De La Fuente, Xia, Branch, & Li, 2013).

Finding alterations in the brain network features associated with pathology is by itself relevant for the characterisation of its pathophysiology. In the case of IUGR, the results suggest that brain reorganisation previously demonstrated in the structural substrate is also present at a functional level since neonatal age. This significantly improves the knowledge of this condition, serving as a potential physiological basis for the neurobehavioral alterations reported in these infants (Figueras et al., 2009). Note that given the heterogeneity of the aetiology and progression of this condition, big samples are needed to find differences in neonatal neurobehavior, being even more crucial to

find individualised biomarkers of the long-term prognosis of infants with IUGR in order to be able to clinically intervene. Although multiple comparisons problems could preclude interpretations of direct partial correlations of network features with NBAS, the ordinal regression of functional network features and NBAS severity score is especially relevant as it is robust to this problem. These results are in line with previous findings reporting an association of network features of structural brain networks with neurodevelopment in IUGR (Batalle et al., 2012; Batalle et al., 2013). In addition, recent reports showing the feasibility to assess functional MRI in fetal period reinforce the potential to use functional brain networks as an early biomarker (Thomason et al., 2013). We are confident that combination of multi-modal features of brain networks will significantly improve the assessment of the risk of neurodevelopmental problems of prenatal origin since an early age, being its translation to the clinical practice in the mid-term horizon.

Finally, there are several issues of the study that must be noted. First, we would like to note that the MRI acquisition was performed during natural sleep. Previous reports have associated deepness of sleep with functional connectivity (Horovitz et al., 2009; Larson-Prior et al., 2009); however, although the effects of sedation and sleep in functional connectivity are not fully understood, significant differences have not been found between sedated and non-sedated infants using ICA and seed-based correlation approaches (Doria et al., 2010; Fransson et al., 2011; Fransson et al., 2009). Importantly, neonatal sleep has been suggested to be mainly in active sleep (Biagioni et al., 2005), minimising the possibility that different sleep deepness could be partially explaining some of the results obtained. Regarding the comparability of the results obtained, two previous studies use ROI-parcellation to study whole brain functional brain networks in neonates (Gao et al., 2011; van den Heuvel et al., 2015). Franson et al. (2011) also assessed whole-brain networks in a neonatal population, however, it was performed voxel-wise in a normalised space, obtaining very large networks (4966-by-4966 elements). Albeit the use of voxel-wise networks has some advantages, constraining the networks obtained to an anatomical brain atlas allows a more comprehensible and manageable comparison among studies, especially given the broad use of AAL atlas in the literature. However, regional parcellation of the neonatal brain is also a critical issue and could be a source of bias. This was alleviated by the use of T2-weighted anatomical

volumes which improve WM contrast in neonates (Williams et al., 2005), and by the use of a specific neonatal atlas (Shi et al., 2011). Note that although we correct for gender in the statistical model, in our population the percentage of males is much higher in IUGR group. Previous studies have described gender-related differences in brain connectivity (Ingalhalikar et al., 2014; Tian, Wang, Yan, & He, 2011), although the specific effects of gender differences on functional brain connectivity at such an early age are still largely unknown. We acknowledge the relatively small sample size available for this study. In order to assess the reliability of the results obtained, we applied a resampling approach allowing us to reassess the differences between cases and controls for global network features. After applying bootstrap with 10000 samples we observed that most of the differences reported are still statistically significant after resampling (Supplementary Table 2). Although the effects associated with IUGR appeared to be consistent when using different approaches, statistical power is limited by this reduced sample size. Further effort to study this very challenging population is needed to confirm the results here presented. With respect of motion during scan, the estimation of motion for both groups was comparable with previously reported for infants and adolescents (Pruim, Mennes, Buitelaar, & Beckmann, 2015), and importantly, we didn't find any significant differences in motion between cases and controls (Table 1), minimising the risk that any of the results reported could be related to different levels of motion in the two groups under study. We acknowledge that the robustness to motion of the approach used to analyse the data, i.e., constructing networks by means of partial correlations within the averaged signal among ROIs, needs to be further assessed (Power, Schlaggar, & Petersen, 2015). However, it should inherently remove signals present throughout the brain, therefore be robust to jerk motion typical in neonatal acquisitions. As the signal of the 88 remaining ROIs is used as a confounder in each of the partial correlations, any signal global to all the brain will be neglected as a possible source of pair-wise correlation. From a specific graph theoretical point of view, partial correlations have been shown to be an effective way to remove head motion effects (Yan, Craddock, He, & Milham, 2013). In addition, the effect of low motion, will also be further compensated by voxel-wise regressing out of the signal the 6 rigid-body features previously used to correct inter-volume motion. We further assessed the effect of motion by adding average FD-RMS and number of frames with high motion

(outliers) as a covariate in the GLM assessing group effects in main network features, without finding any relevant difference with reported results (Supplementary Table 3). Furthermore, we also tested censoring of frames with high motion and regressing them out from correlations when computing connectivity matrices (Supplementary Material), also confirming the main findings reported, suggesting that the motion during acquisition did not have a relevant effect in the graph theory characteristics here reported. Finally, since haemodynamic adaptation in IUGR occurs with blood flow redistribution preferentially to the brain, i.e. the brain sparing effect, we could not discard that part of the changes observed could be related with changes in brain vasculature. Since most of IUGR babies included in our study did not have brain vasodilation, as assessed by Middle Cerebral Artery pulsatility index, we could expect that differences would not be related with changes in neurovasculature. However, early changes in brain blood redistribution could also affect pulsatility index (Garcia-Canadilla et al., 2014), not allowing us to discard this effect in our population.

## 5. CONCLUSIONS

In conclusion, the results presented show the feasibility of using functional brain networks at neonatal age to characterise alterations of prenatal origin. Using IUGR as a model of prenatal condition allowed finding a unique pattern of alterations in the functional brain network organisation, associated with neurobehavioral scores. Overall, the observed functional reorganisation in IUGR neonates could be a potential substrate of altered neurodevelopment in infants with IUGR, and together with previous findings, postulate IUGR condition as a possible brain-network disorder. Association of network features with neurobehavior since neonatal age opens the opportunity to develop early image biomarkers of altered neurodevelopment, a clinical chance to improve the management of a condition that affects up to 10% of the population.

## 6. ACKNOWLEDGEMENTS

The authors would like to thank Cesar Garrido for his help in the design and performance of the acquisition scheme. The images used were acquired in the Magnetic Resonance core facility of Institut d'Investigacions Biomèdiques August Pi I Sunyer (IDIBAPS), Barcelona, Spain. This work was supported by grants from: Obra Social "la Caixa", Barcelona, Spain; The Cerebra Foundation

for the Brain-Injured Child, Carmarthen, Wales, UK; Fundacion Dexeus, Barcelona, Spain; Project PI13/01018 and Sara Borrell grant CD11/00048 to E.M., "Integrado en el Plan Nacional de I+D+I y cofinanciado por el ISCIII-Subdirección General de Evaluación y el Fondo Europeo de Desarrollo Regional (FEDER). Unión Europea. "Otra manera de hacer Europa"".

ACCEPTED MANUSCRIPT

## 7. REFERENCES

- Achard, S., & Bullmore, E. (2007). Efficiency and cost of economical brain functional networks. *PLoS Comput Biol*, 3(2), e17.
- Als, H., Duffy, F. H., McAnulty, G., Butler, S. C., Lightbody, L., Kosta, S., . . . Warfield, S. K. (2012). NICHD improves brain function and structure in preterm infants with severe intrauterine growth restriction. *J Perinatol*, 32(10), 797-803.
- Arcangeli, T., Thilaganathan, B., Hooper, R., Khan, K. S., & Bhide, A. (2012). Neurodevelopmental delay in small babies at term: a systematic review. *Ultrasound Obstet Gynecol*, 40(3), 267-275.
- Ashburner, J., & Friston, K. J. (2005). Unified segmentation. *Neuroimage*, 26(3), 839-851.
- Baschat, A. A. (2013). Neurodevelopment after Fetal Growth Restriction. *Fetal Diagn Ther, E-pub ahead of print*.
- Bassett, D. S., & Bullmore, E. T. (2009). Human brain networks in health and disease. *Curr Opin Neurol*, 22(4), 340-347.
- Batalle, D., Eixarch, E., Figueras, F., Munoz-Moreno, E., Bargallo, N., Illa, M., . . . Gratacos, E. (2012). Altered small-world topology of structural brain networks in infants with intrauterine growth restriction and its association with later neurodevelopmental outcome. *Neuroimage*, 60(2), 1352-1366.
- Batalle, D., Munoz-Moreno, E., Arbat-Plana, A., Illa, M., Figueras, F., Eixarch, E., & Gratacos, E. (2014). Long-term reorganization of structural brain networks in a rabbit model of intrauterine growth restriction. *Neuroimage*, 100, 24-38.
- Batalle, D., Munoz-Moreno, E., Figueras, F., Bargallo, N., Eixarch, E., & Gratacos, E. (2013). Normalization of similarity-based individual brain networks from gray matter MRI and its association with neurodevelopment in infants with intrauterine growth restriction. *Neuroimage*, 83, 901-911.
- Benjamini, Y., Krieger, A. M., & Yekutieli, D. (2006). Adaptive linear step-up procedures that control the false discovery rate. *Biometrika*, 93(3), 491-507.
- Biagioni, E., Boldrini, A., Giganti, F., Guzzetta, A., Salzarulo, P., & Cioni, G. (2005). Distribution of sleep and wakefulness EEG patterns in 24-h recordings of preterm and full-term newborns. *Early Hum Dev*, 81(4), 333-339.
- Biswal, B., Yetkin, F. Z., Haughton, V. M., & Hyde, J. S. (1995). Functional connectivity in the motor cortex of resting human brain using echo-planar MRI. *Magn Reson Med*, 34(4), 537-541.
- Braun, U., Plichta, M. M., Esslinger, C., Sauer, C., Haddad, L., Grimm, O., . . . Meyer-Lindenberg, A. (2011). Test-retest reliability of resting-state connectivity network characteristics using fMRI and graph theoretical measures. *Neuroimage*, 59(2), 1404-1412.
- Bullmore, E., & Sporns, O. (2009). Complex brain networks: graph theoretical analysis of structural and functional systems. *Nat Rev Neurosci*, 10(3), 186-198.
- Cabral, J., Hugues, E., Kringelbach, M. L., & Deco, G. (2012). Modeling the outcome of structural disconnection on resting-state functional connectivity. *Neuroimage*, 62(3), 1342-1353.
- Cabral, J., Kringelbach, M. L., & Deco, G. (2012). Functional graph alterations in schizophrenia: a result from a global anatomic decoupling? *Pharmacopsychiatry*, 45 Suppl 1, S57-64.
- Costas Moragas, C., Fornieles Deu, A., Botet Mussons, F., Boatella Costa, E., & de Caceres Zurita, M. L. (2007). [Psychometric evaluation of the Brazelton Scale in a sample of Spanish newborns]. *Psicothema*, 19(1), 140-149.
- De Bie, H. M., Oostrom, K. J., Boersma, M., Veltman, D. J., Barkhof, F., Delemarre-van de Waal, H. A., & van den Heuvel, M. P. (2011). Global and regional differences in brain anatomy of young children born small for gestational age. *PLoS One*, 6(9), e24116.

- De La Fuente, A., Xia, S., Branch, C., & Li, X. (2013). A review of attention-deficit/hyperactivity disorder from the perspective of brain networks. *Front Hum Neurosci*, *7*, 192.
- Deco, G., Ponce-Alvarez, A., Mantini, D., Romani, G. L., Hagmann, P., & Corbetta, M. (2013). Resting-state functional connectivity emerges from structurally and dynamically shaped slow linear fluctuations. *J Neurosci*, *33*(27), 11239-11252.
- Doria, V., Beckmann, C. F., Arichi, T., Merchant, N., Groppo, M., Turkheimer, F. E., . . . Edwards, A. D. (2010). Emergence of resting state networks in the preterm human brain. *Proc Natl Acad Sci U S A*, *107*(46), 20015-20020.
- Dubois, J., Benders, M., Borradori-Tolsa, C., Cachia, a., Lazeyras, F., Ha-Vinh Leuchter, R., . . . Hüppi, P. S. (2008). Primary cortical folding in the human newborn: an early marker of later functional development. *Brain*, *131*, 2028-2041.
- Egaña-Ugrinovic, G., Sanz-Cortes, M., Figueras, F., Bargallo, N., & Gratacos, E. (2013). Differences in cortical development assessed by fetal MRI in late-onset intrauterine growth restriction. *Am J Obstet Gynecol*, *209*(2), 126 e121-128.
- Esteban, F. J., Padilla, N., Sanz-Cortes, M., de Miras, J. R., Bargallo, N., Villoslada, P., & Gratacos, E. (2010). Fractal-dimension analysis detects cerebral changes in preterm infants with and without intrauterine growth restriction. *Neuroimage*, *53*(4), 1225-1232.
- Figueras, F., Meler, E., Iraola, A., Eixarch, E., Coll, O., Figueras, J., . . . Gardosi, J. (2008). Customized birthweight standards for a Spanish population. *Eur J Obstet Gynecol Reprod Biol*, *136*(1), 20-24.
- Figueras, F., Oros, D., Cruz-Martinez, R., Padilla, N., Hernandez-Andrade, E., Botet, F., . . . Gratacos, E. (2009). Neurobehavior in term, small-for-gestational age infants with normal placental function. *Pediatrics*, *124*(5), e934-941.
- Fischi-Gomez, E., Vasung, L., Meskaldji, D. E., Lazeyras, F., Borradori-Tolsa, C., Hagmann, P., . . . Hüppi, P. S. (2014). Structural Brain Connectivity in School-Age Preterm Infants Provides Evidence for Impaired Networks Relevant for Higher Order Cognitive Skills and Social Cognition. *Cereb Cortex*.
- Fransson, P., Aden, U., Blennow, M., & Lagercrantz, H. (2011). The functional architecture of the infant brain as revealed by resting-state fMRI. *Cereb Cortex*, *21*(1), 145-154.
- Fransson, P., Skiold, B., Engstrom, M., Hallberg, B., Mosskin, M., Aden, U., . . . Blennow, M. (2009). Spontaneous brain activity in the newborn brain during natural sleep--an fMRI study in infants born at full term. *Pediatr Res*, *66*(3), 301-305.
- Fransson, P., Skiold, B., Horsch, S., Nordell, A., Blennow, M., Lagercrantz, H., & Aden, U. (2007). Resting-state networks in the infant brain. *Proc Natl Acad Sci U S A*, *104*(39), 15531-15536.
- Gao, W., Gilmore, J. H., Giovanello, K. S., Smith, J. K., Shen, D., Zhu, H., & Lin, W. (2011). Temporal and spatial evolution of brain network topology during the first two years of life. *PLoS One*, *6*(9), e25278.
- Gao, W., Zhu, H., Giovanello, K. S., Smith, J. K., Shen, D., Gilmore, J. H., & Lin, W. (2009). Evidence on the emergence of the brain's default network from 2-week-old to 2-year-old healthy pediatric subjects. *Proc Natl Acad Sci U S A*, *106*(16), 6790-6795.
- Garcia-Canadilla, P., Rudenick, P. A., Crispi, F., Cruz-Lemini, M., Palau, G., Camara, O., . . . Bijnens, B. H. (2014). A computational model of the fetal circulation to quantify blood redistribution in intrauterine growth restriction. *PLoS Comput Biol*, *10*(6), e1003667.
- Gardener, H., Spiegelman, D., & Buka, S. L. (2011). Perinatal and neonatal risk factors for autism: a comprehensive meta-analysis. *Pediatrics*, *128*(2), 344-355.
- Ginestet, C. E., Nichols, T. E., Bullmore, E. T., & Simmons, A. (2011). Brain network analysis: separating cost from topology using cost-integration. *PLoS One*, *6*(7), e21570.



- Glerean, E., Salmi, J., Lahnakoski, J. M., Jaaskelainen, I. P., & Sams, M. (2012). Functional magnetic resonance imaging phase synchronization as a measure of dynamic functional connectivity. *Brain Connect*, *2*(2), 91-101.
- Hagmann, P. (2005). *From diffusion MRI to brain connectomics.*, Ecole Polytechnique Fédérale de Lausanne (EPFL), Lausanne.
- Heinonen, K., Räikkönen, K., Pesonen, A.-K., Andersson, S., Kajantie, E., Eriksson, J. G., . . . Lano, A. (2010). Behavioural symptoms of attention deficit/hyperactivity disorder in preterm and term children born small and appropriate for gestational age: a longitudinal study. *BMC pediatrics*, *10*, 91.
- Honey, C. J., Sporns, O., Cammoun, L., Gigandet, X., Thiran, J. P., Meuli, R., & Hagmann, P. (2009). Predicting human resting-state functional connectivity from structural connectivity. *Proc Natl Acad Sci U S A*, *106*(6), 2035-2040.
- Horowitz, S. G., Braun, A. R., Carr, W. S., Picchioni, D., Balkin, T. J., Fukunaga, M., & Duyn, J. H. (2009). Decoupling of the brain's default mode network during deep sleep. *Proc Natl Acad Sci U S A*, *106*(27), 11376-11381.
- Illa, M., Eixarch, E., Bataille, D., Arbat-Plana, A., Muñoz-Moreno, E., Figueras, F., & Gratacos, E. (2013). Long-Term Functional Outcomes and Correlation with Regional Brain Connectivity by MRI Diffusion Tractography Metrics in a Near-Term Rabbit Model of Intrauterine Growth Restriction. *PLoS ONE*, *8*(10), e76453.
- Ingalhalikar, M., Smith, A., Parker, D., Satterthwaite, T. D., Elliott, M. A., Ruparel, K., . . . Verma, R. (2014). Sex differences in the structural connectome of the human brain. *Proc Natl Acad Sci U S A*, *111*(2), 823-828.
- Larson-Prior, L. J., Zempel, J. M., Nolan, T. S., Prior, F. W., Snyder, A. Z., & Raichle, M. E. (2009). Cortical network functional connectivity in the descent to sleep. *Proc Natl Acad Sci U S A*, *106*(11), 4489-4494.
- Lin, W., Zhu, Q., Gao, W., Chen, Y., Toh, C. H., Styner, M., . . . Gilmore, J. H. (2008). Functional connectivity MR imaging reveals cortical functional connectivity in the developing brain. *AJNR Am J Neuroradiol*, *29*(10), 1883-1889.
- Linnet, K. M., Wisborg, K., Agerbo, E., Secher, N. J., Thomsen, P. H., & Henriksen, T. B. (2006). Gestational age, birth weight, and the risk of hyperkinetic disorder. *Arch Dis Child*, *91*(8), 655-660.
- Liu, Y., Liang, M., Zhou, Y., He, Y., Hao, Y., Song, M., . . . Jiang, T. (2008). Disrupted small-world networks in schizophrenia. *Brain*, *131*(Pt 4), 945-961.
- Lodygensky, G. A., Seghier, M. L., Warfield, S. K., Tolsa, C. B., Sizonenko, S., Lazeyras, F., & Huppi, P. S. (2008). Intrauterine growth restriction affects the preterm infant's hippocampus. *Pediatr Res*, *63*(4), 438-443.
- Løhaugen, G. C., Østgård, H. F., Andreassen, S., Jacobsen, G. W., Vik, T., Brubakk, A. M., . . . Martinussen, M. (2013). Small for gestational age and intrauterine growth restriction decreases cognitive function in young adults. *J Pediatr*, *163*(2), 447-453.
- Lynall, M. E., Bassett, D. S., Kerwin, R., McKenna, P. J., Kitzbichler, M., Muller, U., & Bullmore, E. (2010). Functional connectivity and brain networks in schizophrenia. *J Neurosci*, *30*(28), 9477-9487.
- Martinussen, M., Flanders, D. W., Fischl, B., Busa, E., Lohaugen, G. C., Skranes, J., . . . Dale, A. M. (2009). Segmental brain volumes and cognitive and perceptual correlates in 15-year-old adolescents with low birth weight. *J Pediatr*, *155*(6), 848-853 e841.
- Maximo, J. O., Cadena, E. J., & Kana, R. K. (2014). The Implications of Brain Connectivity in the Neuropsychology of Autism. *Neuropsychol Rev*.

- McAnulty, G., Duffy, F. H., Kosta, S., Weisenfeld, N. I., Warfield, S. K., Butler, S. C., . . . Als, H. (2013). School-age effects of the newborn individualized developmental care and assessment program for preterm infants with intrauterine growth restriction: preliminary findings. *BMC Pediatr*, *13*, 25.
- Menon, V. (2013). Developmental pathways to functional brain networks: emerging principles. *Trends Cogn Sci*, *17*(12), 627-640.
- Ment, L. R., Hirtz, D., & Huppi, P. S. (2009). Imaging biomarkers of outcome in the developing preterm brain. *Lancet Neurol*, *8*(11), 1042-1055.
- Moore, G. S., Kneitel, A. W., Walker, C. K., Gilbert, W. M., & Xing, G. (2012). Autism risk in small- and large-for-gestational-age infants. *Am J Obstet Gynecol*, *206*(4), 314 e311-319.
- Nielsen, P. R., Mortensen, P. B., Dalman, C., Henriksen, T. B., Pedersen, M. G., Pedersen, C. B., & Agerbo, E. (2013). Fetal growth and schizophrenia: a nested case-control and case-sibling study. *Schizophr Bull*, *39*(6), 1337-1342.
- Nugent, J., & Brazelton, T. (2000). *Preventive mental health: Uses of the Brazelton Scale* (Vol. Vol 2: Early Intervention, Evaluation and Assessment). New York, NY: Wiley.
- Padilla, N., Falcon, C., Sanz-Cortes, M., Figueras, F., Bargallo, N., Crispi, F., . . . Gratacos, E. (2011). Differential effects of intrauterine growth restriction on brain structure and development in preterm infants: a magnetic resonance imaging study. *Brain Res*, *1382*, 98-108.
- Power, J. D., Barnes, K. A., Snyder, A. Z., Schlaggar, B. L., & Petersen, S. E. (2012). Spurious but systematic correlations in functional connectivity MRI networks arise from subject motion. *Neuroimage*, *59*(3), 2142-2154.
- Power, J. D., Schlaggar, B. L., & Petersen, S. E. (2015). Recent progress and outstanding issues in motion correction in resting state fMRI. *Neuroimage*, *105*, 536-551.
- Pruim, R. H., Mennes, M., Buitelaar, J. K., & Beckmann, C. F. (2015). Evaluation of ICA-AROMA and alternative strategies for motion artifact removal in resting state fMRI. *Neuroimage*, *112*, 278-287.
- Rubinov, M., & Bullmore, E. (2013). Fledgling pathoconnectomics of psychiatric disorders. *Trends Cogn Sci*, *17*(12), 641-647.
- Rubinov, M., & Sporns, O. (2009). Complex network measures of brain connectivity: uses and interpretations. *Neuroimage*, *52*(3), 1059-1069.
- Rudie, J. D., Brown, J. A., Beck-Pancer, D., Hernandez, L. M., Dennis, E. L., Thompson, P. M., . . . Dapretto, M. (2012). Altered functional and structural brain network organization in autism. *Neuroimage Clin*, *2*, 79-94.
- Sagiv, S. K., Nugent, J. K., Brazelton, T. B., Choi, A. L., Tolbert, P. E., Altshul, L. M., & Korrick, S. A. (2008). Prenatal organochlorine exposure and measures of behavior in infancy using the Neonatal Behavioral Assessment Scale (NBAS). *Environ Health Perspect*, *116*(5), 666-673.
- Sakoglu, U., Pearlson, G. D., Kiehl, K. A., Wang, Y. M., Michael, A. M., & Calhoun, V. D. (2010). A method for evaluating dynamic functional network connectivity and task-modulation: application to schizophrenia. *MAGMA*, *23*(5-6), 351-366.
- Salvador, R., Suckling, J., Coleman, M. R., Pickard, J. D., Menon, D., & Bullmore, E. (2005). Neurophysiological architecture of functional magnetic resonance images of human brain. *Cereb Cortex*, *15*(9), 1332-1342.
- Sanz-Cortes, M., Ratta, G. A., Figueras, F., Bonet-Carne, E., Padilla, N., Arranz, A., . . . Gratacos, E. (2013). Automatic quantitative MRI texture analysis in small-for-gestational-age fetuses discriminates abnormal neonatal neurobehavior. *PLoS One*, *8*(7), e69595.
- Shi, F., Yap, P. T., Wu, G., Jia, H., Gilmore, J. H., Lin, W., & Shen, D. (2011). Infant brain atlases from neonates to 1- and 2-year-olds. *PLoS One*, *6*(4), e18746.

- Skranes, J. S., Martinussen, M., Smevik, O., Myhr, G., Indredavik, M., Vik, T., & Brubakk, A. M. (2005). Cerebral MRI findings in very-low-birth-weight and small-for-gestational-age children at 15 years of age. *Pediatr Radiol*, *35*(8), 758-765.
- Smith, S. M. (2002). Fast robust automated brain extraction. *Hum Brain Mapp*, *17*(3), 143-155.
- Smyser, C. D., Inder, T. E., Shimony, J. S., Hill, J. E., Degnan, A. J., Snyder, A. Z., & Neil, J. J. (2010). Longitudinal analysis of neural network development in preterm infants. *Cereb Cortex*, *20*(12), 2852-2862.
- Sporns, O., Tononi, G., & Kotter, R. (2005). The human connectome: A structural description of the human brain. *PLoS Comput Biol*, *1*(4), e42.
- Thomason, M. E., Dassanayake, M. T., Shen, S., Katkuri, Y., Alexis, M., Anderson, A. L., . . . Romero, R. (2013). Cross-hemispheric functional connectivity in the human fetal brain. *Sci Transl Med*, *5*(173), 173ra124.
- Tian, L., Wang, J., Yan, C., & He, Y. (2011). Hemisphere- and gender-related differences in small-world brain networks: a resting-state functional MRI study. *Neuroimage*, *54*(1), 191-202.
- Tolsa, C. B., Zimine, S., Warfield, S. K., Freschi, M., Sancho Rossignol, A., Lazeyras, F., . . . Huppi, P. S. (2004). Early alteration of structural and functional brain development in premature infants born with intrauterine growth restriction. *Pediatr Res*, *56*(1), 132-138.
- Tristan-Vega, A., & Arribas, J. I. (2007). *A Fast B-Spline Pseudo-inversion Algorithm for Consistent Image Registration*. Paper presented at the Proceedings of the International Conference on Computer Analysis Images and Patterns (CAIP), Vienna, Austria.
- Tzourio-Mazoyer, N., Landeau, B., Papathanassiou, D., Crivello, F., Etard, O., Delcroix, N., . . . Joliot, M. (2002). Automated anatomical labeling of activations in SPM using a macroscopic anatomical parcellation of the MNI MRI single-subject brain. *NeuroImage*, *15*, 273-289.
- van den Heuvel, M. P., Kersbergen, K. J., de Reus, M. A., Keunen, K., Kahn, R. S., Groenendaal, F., . . . Benders, M. J. (2015). The Neonatal Connectome During Preterm Brain Development. *Cereb Cortex*, *25*(9), 3000-3013.
- Wang, L., Zhu, C., He, Y., Zang, Y., Cao, Q., Zhang, H., . . . Wang, Y. (2009). Altered small-world brain functional networks in children with attention-deficit/hyperactivity disorder. *Hum Brain Mapp*, *30*(2), 638-649.
- Warfield, S. K., Guimond, A., Roche, A., Bharatha, A., Tei, A., Talos, F., . . . Kilkinis, R. (2002). Advanced Nonrigid Registration Algorithms for Image Fusion. In J. C. Mazziotta & A. W. Toga (Eds.), *Brain Mapping: The Methods* (2nd ed., Vol. 24, pp. 661-690): Elsevier.
- Williams, L. A., Gelman, N., Picot, P. A., Lee, D. S., Ewing, J. R., Han, V. K., & Thompson, R. T. (2005). Neonatal brain: regional variability of in vivo MR imaging relaxation rates at 3.0 T--initial experience. *Radiology*, *235*(2), 595-603.
- Xia, M., Wang, J., & He, Y. (2013). BrainNet Viewer: a network visualization tool for human brain connectomics. *PLoS One*, *8*(7), e68910.
- Yan, C. G., Craddock, R. C., He, Y., & Milham, M. P. (2013). Addressing head motion dependencies for small-world topologies in functional connectomics. *Front Hum Neurosci*, *7*, 910.
- Yap, P. T., Fan, Y., Chen, Y., Gilmore, J. H., Lin, W., & Shen, D. (2011). Development trends of white matter connectivity in the first years of life. *PLoS ONE*, *6*(9), e24678.

**FIGURE CAPTIONS**

**Figure 1.** Representation of control and IUGR raw and normalised average functional brain networks (A). Comparison of average strength (B), network density (C), raw global and local efficiency (D) and normalised global and local efficiency (E) between controls and IUGR. Cost-corrected values and its integration in the valid cost range (0.51-0) of binary global efficiency (F), binary local efficiency (G), normalised global efficiency (H) and normalised local efficiency (I). \*  $p < 0.05$ .

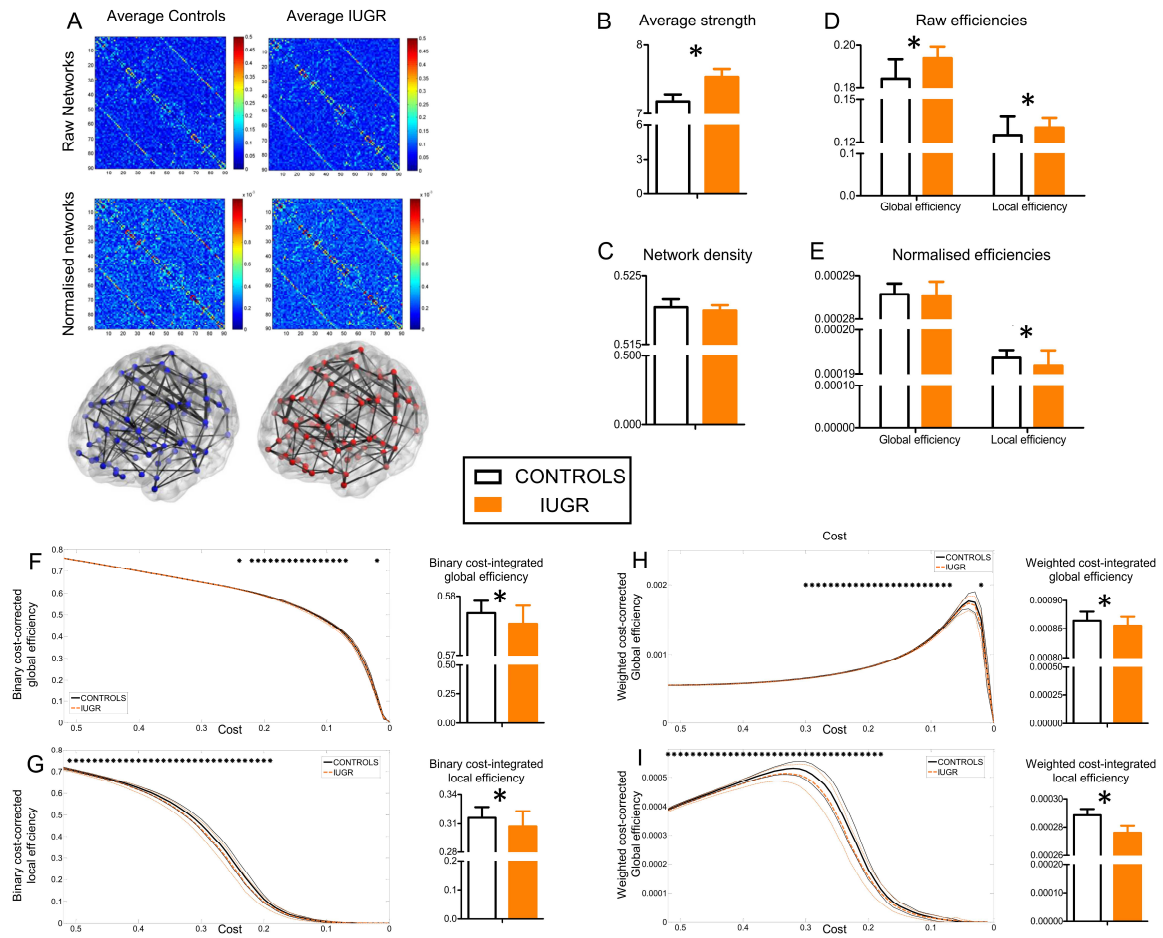
**Figure 2.** Pattern of alterations in IUGR nodal weighted efficiency and nodal strength of raw and normalised networks. Raw features increased (A) and decreased (B) in IUGR group. Normalised features increased (C) and decreased (D) in IUGR group. L and R indicate left and right side of the brain respectively. See correspondence of abbreviations with anatomical regions in Supplementary Table 1.

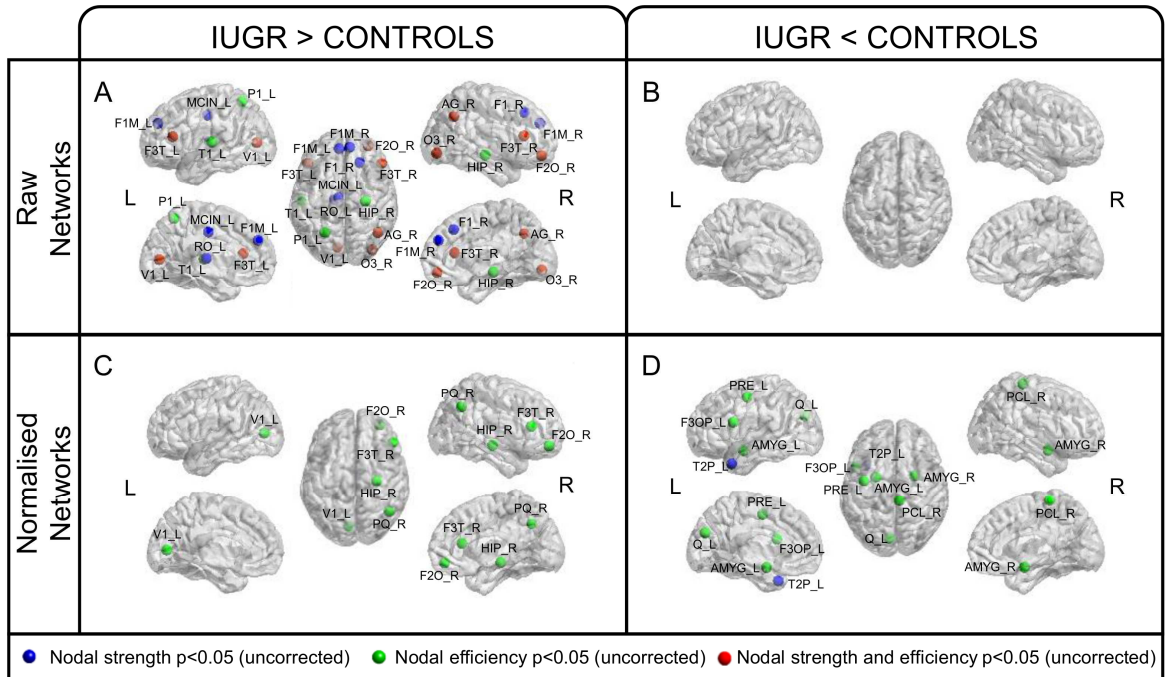
**Figure 3.** Kuramoto order parameter at each time point compared between cases and controls (A). Kuramoto order parameter reordered according to relative value for each subject, from its lowest to its highest value (B). Global (C) and local efficiency (D) at each time point reordered according relative Kuramoto order parameter. Time points where nodal efficiency is significantly different in IUGR when compared with controls and its frequency among time points (E). Red dotted line in panel E is set at 25.1%, corresponding to two standard deviations above average percentage of significant alterations. Regions significantly different during more than 25.1 % are left superior frontal gyrus dorsolateral part (3), right middle frontal gyrus, orbital part (10), right median cingulate and paracingulate gyri (34), and left lingual gyrus (47). See abbreviations of altered regions in Supplementary Table 1.

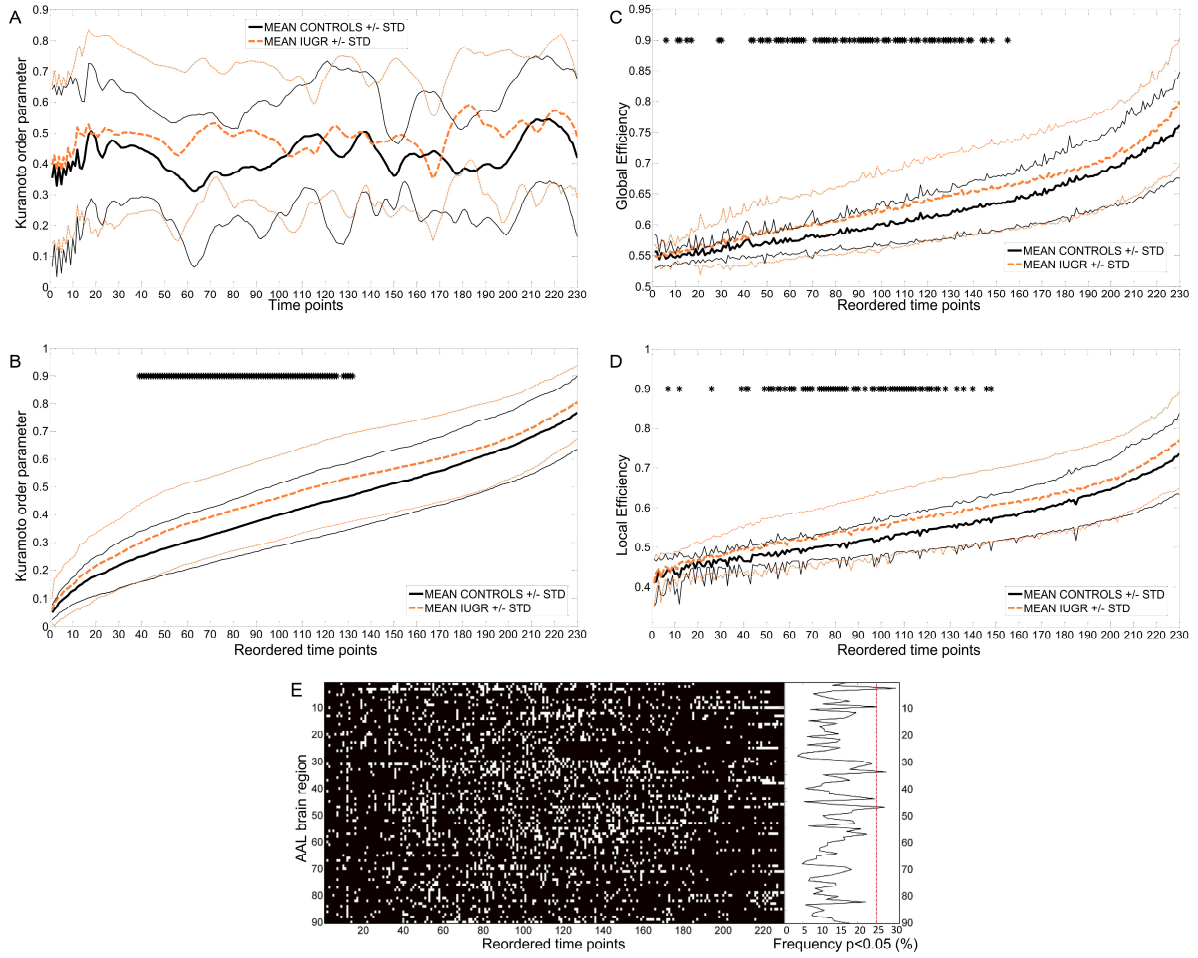
**Table 1.** Neonatal data, demographic characteristics, NBAS results, SAR and motion estimation during scan.

	Controls n=13	IUGR n=20	p <sup>a</sup>
Neonatal data			
GA at delivery [weeks]	39.4 (1.7)	38.2 (2.1)	0.089
Birth weight [g]	3304 (332)	2148 (623)	<b>&lt;0.001</b>
Birth weight centile	54.7 (28.4)	2.1 (2.7)	<b>&lt;0.001</b>
Gender distribution (male/female)	5/8	13/7	0.135
Apgar 5 minutes	10 (0)	9.8 (0.5)	0.255
Umbilical artery pH	7.25 (0.05)	7.23 (0.07)	0.388
Neonatal complications	-	-	-
Demographic characteristics			
Maternal age [years]	35.7 (2.4)	31.9 (4.6)	<b>0.009</b>
Maternal education high school or less	38.5%	40.0%	0.930
Caucasian	61.5%	55.0%	0.710
Smoking during pregnancy	0 %	10 %	0.508
Age at MR (post-menstrual age) [weeks]	44.0 (1.9)	43.0 (2.2)	0.201
NBAS z-scores <sup>b</sup>			
Social interactive <sup>b</sup>	0.37 (2.16)	0.30 (1.53)	0.979
Organization of state <sup>c</sup>	-1.26 (1.61)	0.07 (1.59)	0.087
Regulation of state <sup>c</sup>	-0.55 (1.42)	-0.97 (0.86)	0.198
Autonomous nervous system <sup>c</sup>	1.01 (0.33)	0.22 (0.77)	<b>0.008</b>
Attention <sup>c</sup>	-0.34 (1.30)	-0.53 (1.19)	0.837
NBAS severity score <sup>b, c</sup>	1.69 (1.38)	1.41 (1.37)	0.597
Acquisition parameters and motion estimation			
SAR [W/kg]	0.44 (0.05)	0.42 (0.07)	0.347
Average FD-RMS motion estimation	0.17 (0.09)	0.22 (0.16)	0.328
Number of frame outliers	9.8 (10.4)	14.0 (12.7)	0.320

<sup>a</sup> Student's t-test for independent samples or Pearson's Chi<sup>2</sup> test<sup>b</sup> GLM with GA as co-variable <sup>c</sup> 13 controls vs. 16 IUGR <sup>d</sup> 13 controls vs. 17 IUGR







ACCEPTED